J. Inv. Ill-Posed Problems, Vol. 8, No. 2, pp. 1–31 (2000)

Influence of refraction to the accuracy of a solution for the 2D-emission tomography problem

E. Yu. DEREVTSOV*, R. DIETZ†, A. K. LOUIS†, and T. SCHUSTER†

Received August 13, 1999

Abstract — We suggest two numerical methods for solving a 2D-emission tomography problem. One of them bases on the approach of best approximation, the other is the algorithm of approximate inverse, which represents a stable regularization scheme for linear ill-posed problems. The mathematical model of emission tomography is given by the exponential ray transform (ERT). The aim of this paper is on the one hand a comparison of both methods by applying them on the inversion of the ERT with constant absorption, and on the other hand the investigation of the reconstruction accuracy, if we have some refraction or absorption within the object under consideration. Several numerical test series quantify the influence of refraction and absorption to the solution and answer some questions, which come from related problems.

1. INTRODUCTION

In computerized tomography there exist a number of real processes which cannot be described rigorously without taking into account the phenomenon of deflection of the rays away from straight lines. The problem arises in the framework of ultrasound tomography, geotomography and in other cases, if radiation or waves interact with an inhomogeneous, or anisotropic medium. Although the degree of inhomogeneity is apparently small, the measurements for rather long distances may be considerably different from data, but they can be approximated if we introduce a refraction in our mathematical model.

Throughout this paper we consider the problem of 2D-emission tomography, that means the determination of a source function f by its exponential

*Sobolev Institute of Mathematics, Siberian Branch of Russian Academy of Sciences, Acad. Koptyug prosp. 4, 630090 Novosibirsk, Russia. E-mail: dert@math.nsc.ru

†Fachbereich Mathematik, Universität des Saarlandes, Geb. 36, 66041 Saarbrücken, Germany. E-mails: rainer@num.uni-sb.de, louis@num.uni-sb.de, thomas@num.uni-sb.de

The work was supported by RFBR – DFG grants No. 96-01-00094, 99-01-04007.

ray transform (ERT). Taking into account refraction within the object under consideration we end up with the integral transform $I^\varepsilon : X \to Y$,

$$I^\varepsilon f(x,\xi) = \int_{\tau_-(x,\xi)}^{0} f\big(\gamma_{x,\xi}(t)\big)\, \exp\Big\{ -\int_t^0 \varepsilon\big(\gamma_{x,\xi}(s)\big)\,\mathrm{d}s \Big\}\,\mathrm{d}t \tag{1.1}$$

as data. Here $\gamma_{x,\xi}$ denotes a geodesic line of a Riemannian metric modelling the refraction, X, Y are separable Hilbert spaces and ε is the absorption. In the papers by Hazou – Solmon or Natterer the $\gamma_{x,\xi}$ are straight lines. In particular, in a human body the absorption is caused by tissue. For the reconstruction we propose two algorithms of different type. One of them is the algorithm of best approximation, the other is the approximate inverse, a regularization method for linear ill-posed problems.

Best approximation means that we choose a finite-dimensional subspace $V_M = \operatorname{span}\{\varphi_i, i = 1,\dots,M\} \subset X$ and approximate the data $g = I^\varepsilon f$ in $U_M = I^\varepsilon(V_M) \subset Y$ by solving the corresponding minimizing problem

$$\min_{g_M \in U_M} \|g - g_M\|_Y \tag{1.2}$$

in the meaning of least squares. Supposing g_M to have the representation $g_M = \sum_{i=1}^M c_i^{(M)} I^\varepsilon \varphi_i$, we define $f_M = \sum_{i=1}^M c_i^{(M)} \varphi_i$ as a solution of the reconstruction problem. We obtain the vector of coefficients $c^{(M)} = (c_1^{(M)},\dots,c_M^{(M)})^\top$ by solving a system of linear equations

$$Gc = b$$

where G denotes the Gram matrix corresponding to the basis $\{\varphi_i\}$, that means $G_{ij} = \langle \varphi_i, \varphi_j \rangle_X$. A more detailed formulation of the algorithm can be found in [2].

The approximate inverse introduced in [6] means the evaluation of inner products of the given data $g = I^\varepsilon f$ and a precomputed reconstruction kernel $\psi_\varepsilon(x)$,

$$f(x) \approx \langle g, \psi_\varepsilon(x) \rangle_Y\,. \tag{1.3}$$

The kernel $\psi_\varepsilon(x)$ is determined as a solution of the equation $(I^\varepsilon)^*\psi_\varepsilon(x) = T_1^x e$, where $(I^\varepsilon)^*$ is an adjoint operator of the operator I^ε, and e is a mollifier that approximates Dirac's delta-function: $T_1^x e \approx \delta_x$ with a translation T_1^x. These identifications make the approximation (1.3) obvious. Using a translation invariance of the underlying operator I^ε, we need to calculate the kernel ψ_ε only once, see [6].

The paper is structured as follows. In Section 2 we describe the ERT with refraction under consideration as linear mapping between Hilbert spaces and present some continuity and stability estimates. The two reconstruction algorithms are formulated briefly in Section 3. In a first part we write down the algorithm of best approximation and indicate some details about the implementation. In this paper the basis functions φ_i of V_M are monomials. Some aspects of approximate inverse are derivated in the second part. Furthermore we calculate the needed reconstruction kernel for the ERT with constant absorption ε_0 using the inversion formula for I^{ε_0}

$$f = \frac{1}{4\pi}\,(I^{\varepsilon_0})^*\,R_{\varepsilon_0}^{-1}\,I^{-\varepsilon_0} f$$

with R_{ε_0} the generalized *Riesz-potential*. For varying absorption in a medium the problem is open, since we have no inversion formulas in this case. We finish this section with the reformulation of approximate inverse for I^{ε_0}. Finally in Section 4 numerical experiments are presented. There are two aims we have in mind to pursue. In the first place we compare our two algorithms applying both of them to the X-ray transform ($\varepsilon = 0$), and the ERT ($\varepsilon = \mathrm{const}$). The accuracy of a reconstruction is studied at a third series of computations, and also we assume the rays to be straight lines though there is a refraction within the object. We will see that the algorithm of approximate inverse achieves better results at a high degree of refraction and if the functions are very slowly convergent in the sense given in the appendix, whereas the best approximation is more exact, if the refraction is only small. Note that all computations are performed with exact data. Furthermore with the approximate inverse we have an algorithm of high efficiency with respect to computation time, and with the latter algorithm a flexible one with respect to the degree of the monomials. The deflection of the rays is characterized by geodesics of certain Riemannian metrics.

The paper ends with some conclusions and discussion infered from the numerical tests. In the appendix the functions being reconstructed in the numerical experiments, as well as the Riemannian metrics used therein, are listed.

2. FORMULATION OF THE PROBLEM

We present a short description of the mathematical background of 2D-emission tomography without any proofs. For further details we refer to [2].

We suppose that some bounded domain B of the Eucledian plane $\mathbb{R}^2$ contains a medium with absorption and refraction. The easiest way to describe a phenomenon of refraction is to use the tools of Riemannian metric. The metric is determined if the element of length

$$\mathrm{d}s^2 = g_{ij}(x^1, x^2)\,\mathrm{d}x^i\,\mathrm{d}x^j. \tag{2.1}$$

is known.

Remark 2.1. We use the notation (x^1, x^2) for a point $x \in B$ as well as the notation (x, y) for a point $p \in B$.

Remark 2.2. In formula (2.1) we use the rule of Einstein, i. e. on repeating sub- and super- indices in a monomial the summation from 1 to 2 is assumed.

So the equation (2.1) means

$$\mathrm{d}s^2 = \sum_{i,j=1}^{2} g_{ij}(x^1, x^2)\, \mathrm{d}x^i\, \mathrm{d}x^j.$$

We define a *dissipative Riemanian domain* (B, g) as a pair consisting of our domain B with a strictly convex (with respect to the metric g) boundary ∂B, and *a simple metric* g. Simple metrics have the property to connect any two points of $B \cup \partial B$ by one unique geodesic line. Let ε be any real measurable function. We describe two different approaches to the correct mathematical setting of the problem.

An idea for solving the problem is to select suitable pairs of two Hilbert spaces which guarantee the invertibility of the linear operator under consideration. Note that in this case the problem is well-posed. In particular, the idea is realized in [10] for different linear operators arising in tensor field tomography.

The *exponential ray transform corresponding to the absorption* ε (ERT) is a linear operator

$$I^{\varepsilon} : C^{\infty}(B) \to C^{\infty}(\partial B \times S^1) \tag{2.2}$$

defined by the equation

$$I^{\varepsilon} f(x, \xi) = \int_{\tau_-(x,\xi)}^{0} f\big(\gamma_{x,\xi}(t)\big) \exp\left\{ -\int_t^0 \varepsilon\Big(\gamma_{x,\xi}(s)\Big)\, \mathrm{d}s \right\} \mathrm{d}t. \tag{2.3}$$

Here $x \in \partial B$ denotes a point on the boundary ∂B, ξ is an outer normal vector in the sense of the metric g with respect to the domain B, $\gamma_{x,\xi} : [\tau_-(x,\xi), 0] \to B$ is a maximal geodesic with initial conditions $\gamma_{x,\xi}(0) = x$, $\gamma'_{x,\xi}(0) = \xi$, and $\tau_-(x,\xi)$ is determined by the properties $\gamma_{x,\xi}\Big(\tau_-(x,\xi)\Big) \in \partial B$, and $\gamma_{x,\xi}(t) \in \mathring{B}$ for $t \in \Big(0, \tau_-(x,\xi)\Big)$. Figure 1 below displays some geodesic lines of the CCP- and the CCN-metric. Further details of these metrics can be found in the appendix.

The purpose of emission tomography is to recover a source function f by its ERT $I^{\varepsilon} f$.

The following properties of I^{ε} are proved in [10]:

1) Since $C^{\infty}(B)$, $C^{\infty}(\partial B \times S^1)$ are dense subspaces of $H^s(B)$ and $H^s(\partial B \times S^1)$, respectively, the operator (2.2) has a continuous extension to the bounded operator

$$I^{\varepsilon} : H^{s}(B) \to H^{s}(\partial B \times S^1) \tag{2.4}$$

for every integer $s \geq 0$.

2) The operator $I^{\varepsilon} : H^1(B) \to H^1(\partial B \times S^1)$ is invertible, and for any $f \in H^1(B)$ a stability estimate

$$\|f\|_{L_2(B)} \leq C \|I^{\varepsilon} f\|_{H^1(\partial B \times S^1)} \tag{2.5}$$

holds with a constant C not depending on f.

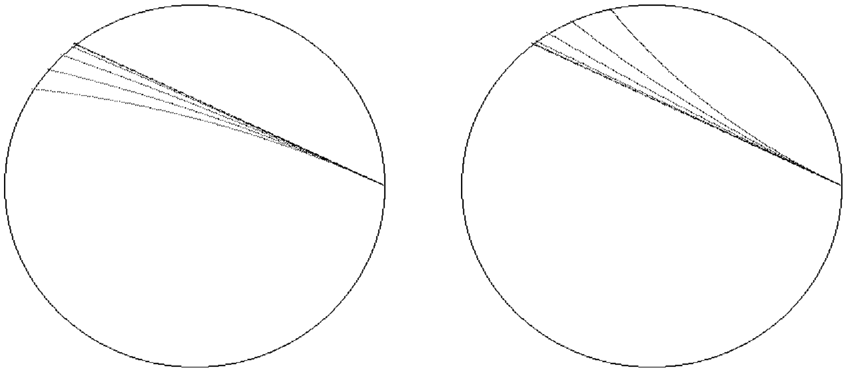

Figure 1: Geodesics of CCP-metric (left), and geodesics of CCN-metric (right) corresponding to the parameters $a = 0.0, 0.1, 0.25, 0.5, 0.75, 1.0$. The values of mean curvatures are $a^2 = 0.0, 0.01, 0.0625, 0.25, 0.56, 1.0$, respectively. The geodesics with $a = 0.0$ and $a = 0.1$ do not differ from each other

We should remember that for validity of these properties some conditions of integral type connecting a tensor of curvature of the metric g with the absorption ε must be valid [2]. In the case of $\varepsilon = 0$ sharper results are known.

The other most commonly used formulation of the problem is motivated by the unavoidable errors in measurements, and reduces to an investigation and solution of the ill-posed integral equation of first order. In this case ERT, corresponding to the absorption $\varepsilon \in L_1(B)$, is regarded as linear operator

$$I^\varepsilon : L_2(B) \to L_2(\partial B \times S^1)\,. \tag{2.6}$$

From now on we assume the domain B to be the unit disk $B = \{x^2 + y^2 \leq 1\}$, which implies $\partial B = S^1$. In case of the euclidean metric according to our assumption on B the formula (2.3) may be written in the more familiar form

$$I^\varepsilon f(\alpha,\beta) = \int_0^{2\cos\beta} f(a+bt, c+dt)\exp\left\{-\int_0^t \varepsilon(a+bs, c+ds)\,\mathrm{d}s\right\}\mathrm{d}t \tag{2.7}$$

arising from fan-beam schemes of observation. Here $f(x,y) \in H^1(B)$, α is a polar angle, $0 \leq \alpha \leq 2\pi$, β is the angle between the normal vector to the circle ∂B at the point $(a,c) = (\cos\alpha, \sin\alpha)$, and the vector $(-b,-d) = (\cos(\alpha+\beta), \sin(\alpha+\beta))$, $-\pi/2 < \beta < \pi/2$ defining the direction of the ray under consideration.

3. NUMERICAL SOLUTION FOR THE PROBLEM WITH REFRACTION UNDER CONSIDERATION

3.1. Algorithm of least squares

At first we briefly describe the general scheme of best approximation. Let us consider separable Hilbert spaces $H^1(B)$, $L_2(B)$, and $H^1(S^1 \times S^1)$. The injection $H^1(B) \subset L_2(B)$ is continuous, and its image is dense in $L_2(B)$. For the operator I^ε the estimates (2.5) and

$$\|I^\varepsilon f\|_{H^1(S^1\times S^1)} \le C_1 \|f\|_{H^1(B)} \tag{3.1}$$

with $f \in H^1(B)$ are valid. For real functions $f, g \in C^\infty(S^1 \times S^1)$ an inner product

$$\langle f, g\rangle_s = \sum_{k,l=-\infty}^{\infty} (1 + k^2 + l^2)^s \, c_{k,l}(f)\, \overline{c_{k,l}(g)} \tag{3.2}$$

is defined, which can be extended to the Sobolev space $H^S\left(S^1 \times S^1\right)$. In (3.2) the values $c_{k,l}(f)$, $c_{k,l}(g)$ are the Fourier coefficients of the functions f and g, respectively. They can be calculated by the formula

$$c_{k,l}(f) = \frac{1}{4\pi^2}\int_0^{2\pi}\int_0^{2\pi} f(\alpha,\beta)\mathrm{e}^{-\mathrm{i}(k\alpha+l\beta)}\,\mathrm{d}\alpha\,\mathrm{d}\beta \qquad (-\infty < k,\ l < \infty) \tag{3.3}$$

The inner product (3.2) can be evaluated very efficiently. In the first place we do not compute the partial derivatives of the functions f, g, if we exploit (3.2) instead of the standard inner products in Sobolev spaces. But it also states that errors in high frequencies, i. e. large $|k|$, $|l|$, are strongly amplified. Secondly formula (3.3) allows us to use the techniques of fast Fourier transform (FFT).

Assume that $I^\varepsilon f = g$ is solvable for some element $g \in H^1\left(S^1 \times S^1\right)$ and we have an approximation g_δ of g such that the inequality

$$\|g_\delta - g\|_{H^1(S^1\times S^1)} = \|g_\delta - I^\varepsilon f\|_{H^1(S^1\times S^1)} < \delta, \tag{3.4}$$

holds. The problem is to find an approximate solution f_δ of the required f. In the space $H^1(B)$ we choose a complete, linear independent sequence of elements

$$\begin{gathered}\varphi_1 = 1, \qquad \varphi_2 = x, \qquad \varphi_3 = y, \qquad \ldots, \qquad \varphi_k = x^n \\ \varphi_{k+1} = x^{n-1}y, \qquad \ldots, \qquad \varphi_{k+n} = y^n, \qquad \ldots\end{gathered} \tag{3.5}$$

which is complete in $L_2(B)$ as well and induces a linear independent sequence

$$\begin{gathered}\psi_1 = I^\varepsilon 1, \qquad \psi_2 = I^\varepsilon x, \qquad \psi_3 = I^\varepsilon y, \qquad \ldots, \qquad \psi_k = I^\varepsilon x^n \\ \psi_{k+1} = I^\varepsilon x^{n-1}y, \qquad \ldots, \qquad \psi_{k+n} = I^\varepsilon y^n, \qquad \ldots\end{gathered} \tag{3.6}$$

in the space $H^1\left(S^1 \times S^1\right)$. For a fixed M we set $g_{\delta_M} = \sum_{k=1}^M c_k^{(M)}\psi_k$. If the coefficients $c_k^{(M)}$ minimizing the norm

$$\|g_\delta - g_{\delta_M}\|_{H^1(S^1\times S^1)} \tag{3.7}$$

are found, then due to the linearity of I^ε and (3.6) we have the equations

$$g_{\delta_M} = \sum_{k=1}^M c_k^{(M)}\psi_k = \sum_{k=1}^M c_k^{(M)} I^\varepsilon\varphi_k = I^\varepsilon\left(\sum_{k=1}^M c_k^{(M)}\varphi_k\right) = I^\varepsilon f_{\delta_M} \tag{3.8}$$

where

$$f_{\delta_M} = \sum_{k=1}^{M} c_k^{(M)} \varphi_k \,. \tag{3.9}$$

It is easy to see that $\|f - f_{\delta_M}\|_{L_2(B)} \to 0$ while $\delta_M \to 0$, $M \to \infty$ is a consequence of the estimates (2.5), inequality (3.4), where the data error is measured in a rather strong norm, and formula (3.8).

The problem of minimizing the norm (3.7) is solved by a least squares method that implies the following system of linear equations:

$$\left.\begin{array}{c} c_1^{(M)}\langle\psi_1,\psi_1\rangle + c_2^{(M)}\langle\psi_1,\psi_2\rangle + \ldots + c_M^{(M)}\langle\psi_1,\psi_M\rangle = \langle g_\delta,\psi_1\rangle \\ c_1^{(M)}\langle\psi_2,\psi_1\rangle + c_2^{(M)}\langle\psi_2,\psi_2\rangle + \ldots + c_M^{(M)}\langle\psi_2,\psi_M\rangle = \langle g_\delta,\psi_2\rangle \\ \cdots\cdots\cdots \\ c_1^{(M)}\langle\psi_M,\psi_1\rangle + c_2^{(M)}\langle\psi_M,\psi_2\rangle + \ldots + c_M^{(M)}\langle\psi_M,\psi_M\rangle = \langle g_\delta,\psi_M\rangle \end{array}\right\} \tag{3.10}$$

Here, $\langle\,\cdot\,,\,\cdot\,\rangle$ denotes the inner product in $H^1\left(S^1 \times S^1\right)$. Since the determinant of the arising Gram matrix is not equal to zero for any M, the system (3.10) has a unique solution, and the coefficients $c_k^{(M)}$ in (3.9) minimizing the norm (3.7) are uniquely determined as well.

Remark 3.1. The main computational tools we use in the algorithm are the following:

1) Fast Fourier transform (FFT) is applied for the calculation of the coefficients $c_{k,l}(f)$ of the inner products (3.2).

2) All elements of the sequence (3.6) are computed simultaneously at a current point of geodesic, and an integration along the geodesic line is produced by a quadrature formula of Bode with the accuracy $O(h^6)$ per step.

3) The system of differential equations for the geodesics leads to an equivalent system of first order, and the latter is solved by a Runge–Kutta method of fourth order of accuracy per step.

The algorithm described above may be useful for a set of problems concerning the inversion of linear operators, as well as for linear problems, which appear in integral geometry. For further details see [2, 10].

3.2. Algorithm of approximate inverse

3.2.1. Some aspects of approximate inverse

Let $A : L_2(\Omega_1) \to L_2(\Omega_2)$ be a linear, injective and bounded operator, $\Omega_i \subset \mathbb{R}^{n_i}$ are assumed to be bounded domains, $i = 1, 2$. For given $g \in L_2(\Omega_2)$ we search a solution for

$$Af = g \,. \tag{3.11}$$

Further we consider a mollifier $e \in L_2(\Omega_1)$, which means

$$\int_{\mathbb{R}^{n_1}} e(x)\, \mathrm{d}x = 1 \tag{3.12}$$

$$\lim_{\gamma\to 0} \gamma^{-n_1} \int_{\mathbb{R}^{n_1}} f(x)\, e\Big(\frac{x-y}{\gamma}\Big)\, \mathrm{d}x = f(y) \qquad \text{a.e.} \tag{3.13}$$

If $e \in$ range (A^*), there exists a $\psi \in L_2(\Omega_2)$ with

$$A^*\psi = e\,. \tag{3.14}$$

With A^* we denote the adjoint operator of A. We define a translation T_1^x on $L_2(\Omega_1)$ by

$$T_1^x f(y) = \gamma^{-n_1}\, f\Big(\frac{y-x}{\gamma}\Big) \quad \text{for} \quad \gamma > 0\,. \tag{3.15}$$

Equation (3.15) together with (3.12) and (3.13) implies $T_1^x e \approx \delta_x$. Let T_2^x be a further translation on $L_2(\Omega_2)$ fulfilling

$$T_1^x A^* = A^* T_2^x\,. \tag{3.16}$$

The idea of approximate inverse is to compute the moments

$$\langle f, T_1^x e\rangle_{L_2(\Omega_1)} \approx f(x) \tag{3.17}$$

instead of f itself. With the assumptions made above we have

$$\begin{aligned}\langle f, T_1^x e\rangle_{L_2(\Omega_1)} &= \langle f, T_1^x A^*\psi\rangle_{L_1(\Omega_1)} = \langle f, A^* T_2^x\psi\rangle_{L_2(\Omega_1)} \\ &= \langle Af, T_2^x\psi\rangle_{L_2(\Omega_2)} = \langle g, T_2^x\psi\rangle_{L_2(\Omega_2)}\end{aligned}$$

see [6]. Here we used (3.11) and (3.16). So, we only have to compute inner products of a translated, precomputed kernel $T_2^x\psi$ with the data g. If $e \notin$ range (A^*), the injectivity of A implies the existence of ψ_ρ with

$$\|A^*\psi_\rho - e\|_{L_2(\Omega_1)} < \rho \tag{3.18}$$

for a given $\rho > 0$.

In the case that A is a compact operator, one possibility to get the kernel ψ is given by the singular value decomposition (SVD) $\{v_\mu, u_\mu, \sigma_\mu\}_\mu$ of A. That means that $\{v_\mu\}_\mu$ is a complete orthonormal system (CONS) of $L_2(\Omega_1)$, $\{u_\mu\}_\mu$ is a CONS of $\overline{\text{range}\,(A)}$ and both of the equations

$$Av_\mu = \sigma_\mu u_\mu\,, \qquad A^* u_\mu = \sigma_\mu v_\mu \tag{3.19}$$

are fulfilled. For given $e \in$ range (A^*) the kernel ψ is represented by

$$\psi = \sum_{\sigma_\mu > 0}^{\infty} \sigma_\mu^{-1}\, \langle e, v_\mu\rangle_{L_2(\Omega_1)}\, u_\mu\,. \tag{3.20}$$

If $e \in L_2(\Omega_1)\setminus$ range (A^*) we get ψ_ρ from (3.18) by cutting the series (3.20) after finitely many steps

$$\psi_\rho = \sum_{\sigma_\mu > 0}^{M_\rho} \sigma_\mu^{-1}\, \langle e, v_\mu\rangle_{L_2(\Omega_1)}\, u_\mu\,. \tag{3.21}$$

M_ρ is chosen accordingly to (3.18). Another approach to obtain reconstruction kernels bases on the inversion formula of the underlying operator A. If the inversion formula has the form

$$f = A^* Q f \tag{3.22}$$

where $Q : \mathsf{D}(Q) \subset L_2(\Omega_1) \to L_2(\Omega_2)$ is a linear mapping with domain $\mathsf{D}(Q)$, a reconstruction kernel ψ for a mollifier e is calculated by

$$\psi = Qe \tag{3.23}$$

where e must fulfill the condition $e \in \mathsf{D}(Q)$. The inversion formula of I^{ε_0} with ε_0 constant is structured like (3.22). So, we will calculate the kernel for I^{ε_0} using (3.23).

We now briefly describe the situation in the semi-discrete case, which is the important case in practical applications. Suppose $X_1 \hookrightarrow L_2(\Omega_1)$ and $Y_1 \hookrightarrow L_2(\Omega_2)$ to be dense subspaces with continuous injections and $A : X_1 \to Y_1$ to be also continuous. The point evaluations $\phi_n : Y_1 \to \mathbb{R}^n$ are defined via

$$(\phi_n g)_i = g(x_i)\,, \qquad \text{with} \quad x_i \in \Omega_2 \quad \text{for} \quad i = 1, \dots, n\,. \tag{3.24}$$

Instead of (3.11) we consider the equation

$$A_n f := \psi_n A f = g_n \tag{3.25}$$

for given $g_n \in \mathbb{R}^n$, and search for a solution $f \in X_1$ of (3.25) by applying the approximate inverse. Since A_n is not continuous on $L_2(\Omega_1)$, we have

$$\mathsf{D}(A_n^*) = \{g \in L_2(\Omega_2) : f \mapsto \langle A_n f, g\rangle_{L_2(\Omega_2)} \text{ is contiuous } \forall f \in X_1\}$$

is a proper subspace of Y. In the worst case we even have $\mathsf{D}(A_n^*) = \{0\}$, that means A_n^* does not exist. This situation occurs for $A = I^\varepsilon$. Furthermore we cannot define a reconstruction kernel for A_n w.r.t. a mollifier e. A way out of this difficulty is shown in [9]. We compute a kernel ψ for the continuous Operator A as we described before, and take

$$\alpha_n(x) := \phi_n \, T_2^x \, \psi \tag{3.26}$$

as reconstruction kernel for A_n. When we use $\alpha_n(x)$ as kernel, a weak convergence of the connected approximate inverse to moments of f can be shown, see [9]. For further investigations we refer to [6, 7, 9].

3.2.2. A reconstruction kernel for I^{ε_0}

For the application of approximate inverse to the ERT we consider I^{ε_0} to be a mapping between $L_2(B)$ and $L_2(S^1 \times (-1,1))$

$$I^{\varepsilon_0} f(\omega, s) = \int\limits_{-\sqrt{1-s^2}}^{\sqrt{1-s^2}} f(s\omega + t\omega^\perp)\, \mathrm{e}^{-\varepsilon_0 t}\, \mathrm{d}t$$

where $\omega(\varphi) = (\cos\varphi, \sin\varphi)^\top$ and $\omega(\varphi)^\perp = (-\sin\varphi, \cos\varphi)^\top$ denote elements of S^1. As we mentioned above, we have in mind to use the inversion formula for I^{ε_0}, see [8, Chapter II.6],

$$e = (I^{\varepsilon_0})^* R_{\varepsilon_0}^{-1} I^{-\varepsilon_0} e, \qquad e \in H_0^\beta(B), \qquad \beta \geq 1/2 \tag{3.27}$$

with a constant $\varepsilon_0 \in \mathbb{R}^+$ for calculating a reconstruction kernel. The operator $R_{\varepsilon_0}^{-1} : H_0^1(-1,1) \to L_2(\mathbb{R})$ is the generalized *Riesz-potential*

$$(R_{\varepsilon_0}^{-1} g)\hat{}(\sigma) = \begin{cases} |\sigma|\, \hat{g}(\sigma) & |\sigma| > \varepsilon_0 \\ 0 & \text{otherwise.} \end{cases}$$

Obviously (3.27) has the form (3.22) with $Q = Q^{\varepsilon_0} = (4\pi)^{-1} R_{\varepsilon_0}^{-1} I^{-\varepsilon_0}$. If $e \in H_0^\beta(B)$, $\beta \geq 1/2$, then $e \in \mathsf{D}(Q^{\varepsilon_0})$. We choose the Gaussian $e(x) = (2\pi)^{-1}\gamma^{-2}\exp(-\gamma^{-2}\|x\|^2/2)$, $\gamma > 0$ as mollifier. For γ arbitrarily small, we can consider e as an element of $H_0^{1/2}(B)$. From (3.23) and from the projection theorem for I^{ε_0}

$$(I^{\varepsilon_0} f)\hat{}(\omega, \sigma) = (2\pi)^{1/2}\, \hat{f}(\sigma\omega - \mathrm{i}\varepsilon_0\omega^\perp)$$

see [8, Chapter II.6], we deduce

$$\begin{aligned}
\psi_{\varepsilon_0}(s) &= Q^{\varepsilon_0} e = (4\pi)^{-1} R_{\varepsilon_0}^{-1} I^{-\varepsilon_0} e = \frac{1}{4\pi}\frac{1}{\sqrt{2\pi}} \int_{\mathbb{R}} \Big(R_{\varepsilon_0}^{-1} I^{-\varepsilon_0} e \Big)\hat{}(\sigma)\, \mathrm{e}^{\mathrm{i}s\sigma}\, \mathrm{d}\sigma \\
&= \frac{1}{4\pi}\frac{1}{\sqrt{2\pi}} \int_{|\sigma|>\varepsilon_0} |\sigma|\, (I^{-\varepsilon_0} e)\hat{}(\sigma)\, \mathrm{e}^{\mathrm{i}s\sigma}\, \mathrm{d}\sigma \\
&= \frac{1}{4\pi} \int_{|\sigma|>\varepsilon_0} |\sigma|\, \hat{e}(\sigma\omega_0 + \mathrm{i}\varepsilon_0\omega_0^\perp)\, e^{\mathrm{i}s\sigma}\, \mathrm{d}\sigma \\
&= \frac{1}{4\pi^2} \int_{\varepsilon_0}^\infty \sigma \exp\Big(-\frac{\gamma^2(\sigma^2 + \varepsilon_0^2)}{2} \Big) \cos(s\sigma)\, \mathrm{d}\sigma \\
&= \frac{-\gamma^{-2}}{4\pi^2} \exp\Big(-\frac{\gamma^2\varepsilon_0^2}{2} \Big) \int_{\varepsilon_0}^\infty \frac{\partial}{\partial\sigma}\Big(\exp\Big(-\frac{\gamma^2\sigma^2}{2} \Big) \Big) \cos(s\sigma)\, \mathrm{d}\sigma.
\end{aligned}$$

An integration by parts yields

$$\begin{aligned}
\psi_{\varepsilon_0}(s) = {} & \frac{\gamma^{-2}}{4\pi^2} \exp\Big(-\frac{\gamma^2\varepsilon_0^2}{2} \Big) \\
& \times \Bigg(\exp\Big(-\frac{\gamma^2\varepsilon_0^2}{2} \Big) \cos(s\varepsilon_0) - s \int_{\varepsilon_0}^\infty \exp\Big(-\frac{\gamma^2\sigma^2}{2} \Big) \sin(s\sigma)\, \mathrm{d}\sigma \Bigg).
\end{aligned}$$

It remains the calculation of the latter integral. We have

$$\begin{aligned}
\int_{\varepsilon_0}^\infty \exp\Big(-\frac{\gamma^2\sigma^2}{2} \Big) \sin(s\sigma)\, \mathrm{d}\sigma = {} & \int_0^\infty \exp\Big(-\frac{\gamma^2\sigma^2}{2} \Big) \sin(s\sigma)\, \mathrm{d}\sigma \\
& - \int_0^{\varepsilon_0} \exp\Big(-\frac{\gamma^2\sigma^2}{2} \Big) \sin(s\sigma)\, \mathrm{d}\sigma
\end{aligned}$$

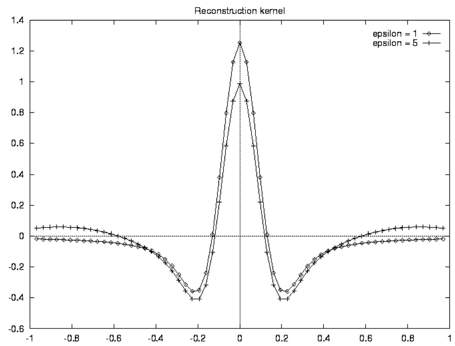

Figure 2: Plot of ψ_{ε_0} for $\varepsilon_0 = 1.0$ (marked with squares), and $\varepsilon_0 = 5.0$ (marked with crosses). Note the positivity of ψ_5 outside the interval $[-0.6, 0.6]$. The kernel $\psi_{0.1}$ would not differ from ψ_1.

and

$$\int_0^\infty \exp\Big(-\frac{\gamma^2\sigma^2}{2}\Big)\sin(s\sigma)\,\mathrm{d}\sigma = \frac{1}{\gamma}\sqrt{\frac{\pi}{2}}\exp\Big(-\frac{s^2}{2\gamma^2}\Big)\,\mathrm{i}\,\mathrm{erf}\Big(-i\,\frac{s}{\sqrt{2}\,\gamma}\Big).$$

Here we used formulas (7.4.7) and (7.1.3) from [1], $\mathrm{erf}(t) = (2/\sqrt{\pi})\int_0^t \exp(-z^2)\,\mathrm{d}z$ is the error function. Unfortunately we are not able to calculate the integral

$$\int_0^{\varepsilon_0} \exp\Big(-\frac{\gamma^2\sigma^2}{2}\Big)\sin(s\sigma)\,\mathrm{d}\sigma =: F_{\gamma,\varepsilon_0}(s) \tag{3.28}$$

exactly. Thus, in applications we approximate (3.28) numerically. Finally the reconstruction kernel ψ_{ε_0} has the representation

$$\begin{aligned}\psi_{\varepsilon_0}(s) = \frac{\gamma^{-2}}{4\pi^2}\exp\Big(-\frac{\gamma^2\varepsilon_0^2}{2}\Big)\Big(&\exp\Big(-\frac{\gamma^2\varepsilon_0^2}{2}\Big)\cos(s\varepsilon_0)\\ &- s\Big(\frac{1}{\gamma}\sqrt{\frac{\pi}{2}}\exp\Big(-\frac{s^2}{2\gamma^2}\Big)\mathrm{i}\,\mathrm{erf}\Big(\mathrm{i}\,\frac{s}{\sqrt{2}\gamma}\Big) + F_{\gamma,\varepsilon_0}(s)\Big)\Big).\end{aligned} \tag{3.29}$$

Remark 3.2. Since $F_{\gamma,\varepsilon_0}(s) = 0$ for $\varepsilon_0 = 0$, we obtain the well known reconstruction kernel for the *2D-Radon transform* w.r.t. the mollifier e in this case, see [9].

Figure 2 displays ψ_{ε_0} for different values of ε_0. As can be seen we obtain a reconstruction kernel similar to the *Shepp – Logan filter* for the Radon transform for small values of ε_0. For a large degree of absorption, for example $\varepsilon_0 = 5$, we see that the kernel ψ_{ε_0} is positive outside some interval $[-\varkappa, \varkappa]$.

3.2.3. Approximate inverse for the ERT I^{ε_0}

We define the translation $T_1^x : L_2(B) \to L_2(B)$ from (3.15) for $f \in L_2(B)$ with $\gamma = 2$ by

$$T_1^x f(y) = \frac{1}{4} f\Big(\frac{y-x}{2}\Big) .$$

The adjoint $(I^{\varepsilon_0})^* : L_2(S^1 \times (-1,1)) \to L_2(B)$ has the representation

$$(I^{\varepsilon_0})^* g(x) = \int_{S^1} g(\omega, \langle x, \omega\rangle)\, \mathrm{e}^{-\varepsilon_0 \langle x, \omega^\perp\rangle}\, \mathrm{d}\omega$$

see [8, Chapter II.6]. A straightforward computation shows, that the translation $T_{2,\varepsilon_0}^x : L_2(S^1 \times (-1,1)) \to L_2(S^1 \times (-1,1))$

$$T_{2,\varepsilon_0}^x g(\omega, s) = \frac{1}{4}\, \mathrm{e}^{\varepsilon_0 \langle x, \omega^\perp\rangle}\, g\Big(\omega, \frac{s - x^\top \omega}{2}\Big)$$

fulfills (3.16) with $A = I^{\varepsilon_0}$, more precisely:

$$T_1^x (I^{\varepsilon_0})^* = (I^{\varepsilon_0})^* T_{2,\varepsilon_0}^x .$$

Hence the approximate inverse of I^{ε_0} is calculated as follows

$$\langle g, T_{2,\varepsilon_0}^x \psi_{\varepsilon_0}\rangle_{L_2(S^1\times(-1,1))} = \frac{1}{4}\int_{S^1}\int_{-1}^{1} g(\omega, s)\, \mathrm{e}^{\varepsilon_0 \langle x, \omega^\perp\rangle}\, \psi_{\varepsilon_0}\Big(\frac{s - x^\top\omega}{2}\Big)\, \mathrm{d}s\, \mathrm{d}\omega$$

with $g = I^{\varepsilon_0} f$.

For a reformulation of the approximate inverse in the fan-beam geometry we use the same arguments as for the Radon transform, see [8, Chapter V.1.2].

4. NUMERICAL EXPERIMENTS

In this section we compare the two reconstruction methods described before by applying them to three different problems. First we reconstruct functions by their X-ray transform in fan-beam geometry. Furthermore we deal with ERT of the source functions as data. Finally, in the third part we calculate the ray transform of the source functions along geodesic lines corresponding to several Riemannian metrics and reconstruct them under the assumption, that the rays are straight lines. For each problem we take four source functions (F.1–F.4), listed in the apppendix.

4.1. X-ray tomography problem

The purpose of the first set of tests is the “graduation” of the algorithms, i.e. the investigation of their behavior in the well known situation of X-ray tomography. Since $\varepsilon = 0$, formula (2.7) has the simple form

$$(If)(\alpha, \beta) = \int_0^{2\cos\beta} f(a + bt, c + dt)\, \mathrm{d}t\,. \tag{4.1}$$

	Best Approximation						Appr. Inv.
sst M	12 91	13 105	14 120	15 136	16 153	17 171	γ 0.02
F.1	0.151	0.063	0.017	0.008	0.001	0.001	6.34
F.2	1.87	1.40	0.67	0.35	0.29	0.13	7.41
F.3	5.56	4.56	3.51	2.28	1.89	0.94	8.04
F.4	23.52	20.56	17.10	12.37	11.28	6.91	14.12

Table 1: Relative errors in % in the reconstruction of the source functions (F.1–F.4) by the best approximation and the approximate inverse (right column) with $N = 64$

Step 1 (Direct problem). We calculate the X-ray transform (ray transform) of the density function $f(x, y)$ at the points $(k\Delta\alpha, \beta_0 - l\Delta\beta)$, where $k = 0, 1, \ldots, N-1$, $\beta_0 = \pi/2$, $l = 1, 2, \ldots, N/2 - 1$. Obviousely we have $If(\alpha_k, \beta_0) = If(\alpha_k, \beta_{N/2}) = 0$. Let $\Delta\alpha = \Delta\beta = 2\pi/N$ be the discretization step sizes.

Step 2 (Inverse problem). We reconstruct the density function by its known (from Step 1) X-ray transform by applying: a) the algorithm of least squares method, b) the algorithm of approximate inverse.

As for a): With sst we denote the maximal degree of the monomials generating the basis of V_M, M is the dimension of V_M.

As for b): For applying the algorithm of approximate inverse it remains to define the observation functionals ϕ_n from (3.24). Let $Y_1 = H^\beta(S^1 \times S^1)$, $Y_2 = H^\beta(S^1 \times (-1, 1))$ and $X_1 = H^{\beta - 1/2}(B)$ with $\beta > 1$. Then we have the boundedness of $I : X_1 \to Y_1$ and $I : X_1 \to Y_2$, respectively. The functionals $\phi_n^1 : Y_1 \to \mathbb{R}^n$ and $\phi_n^2 : Y_2 \to \mathbb{R}^n$, $n = N(N/2 - 1)$, are defined by

$$(\phi_n^1 g)_{kl} = g(\alpha_k, \beta_l) \tag{4.2}$$

$$(\phi_n^2 g)_{kl} = g(\omega(\alpha_k + \beta_l - \pi/2), \sin\beta_l)\,. \tag{4.3}$$

They induce the semi-discrete operator $I_n = \phi_n^1\, I$ and the reconstruction kernel $\alpha_n(x) = \phi_n^2\, T_{2,0}^x \psi_0$. The approximate inverse is computed as follows:

$$f(x) \approx \langle \phi_n^1\, If, \alpha_n(x) \rangle_{\mathbb{R}^n}\,.$$

With γ we denote the regularization parameter appearing in the representation (3.29) of ψ_0.

The computation time of the approximate inverse on a SGI Challenge was about 0.8 seconds per function. That means, that we have a very efficient algorithm, which is suitable also for data sets of large size. In contrast, the best approximation is flexible in the sense of choosing the number of basis functions φ_i. As for the worse accuracy in case of approximate inverse, see Remark 4.1.

4.2. Emission tomography problem with a constant absorption

The following series of numerical tests pursues the aim of investing the algorithms under the condition, that the degree of absorption increasis and therefore the "intensity of a signal" decreasis. By "intensity of a signal" we mean the ERT as a function depending on two angle variables α, β. Formula (2.7) has the form

$$I^{\varepsilon_0} f(\alpha,\beta) = \int_0^{2\cos\beta} f(a+bt, c+dt)\, \mathrm{e}^{-\varepsilon_0 t}\, \mathrm{d}t \tag{4.4}$$

in this case.

Step 1 (Direct problem). ERT with constant absorption ε_0 of the function $f(x,y)$ is calculated by formula (4.4) at the same points $(k\Delta\alpha, \beta_0 - l\Delta\beta)$, $k = 0,1,\ldots,N-1$, $\beta_0 = \pi/2$, $l = 1,2,\ldots,N/2-1$. Here,$\Delta\alpha = \Delta\beta = 2\pi/N$ are again the discretization step sizes.

Step 2 (Inverse problem). We reconstruct the source function $f(x,y)$ by its known attenuated ray transform by applying: a) the algorithm of approximate inverse; b) the algorithm of best approximation.

Let $\phi_n^1 : Y_1 \to \mathbb{R}^n$, $\phi_n^2 : Y_2 \to \mathbb{R}^n$, $n = N(N/2-1)$ be defined as in (4.2) and (4.3), respectively. They induce the semi-discrete operator $I_n^{\varepsilon_0} = \phi_n^1 I^{\varepsilon_0}$ and the reconstruction kernel $\alpha_n^{\varepsilon_0}(x) = \phi_n^2 T^x_{2,\varepsilon_0}\psi_{\varepsilon_0}$. The approximate inverse is computed as follows

$$f(x) \approx \langle \phi_n^1 I^{\varepsilon_0} f, \alpha_n^{\varepsilon_0}(x)\rangle_{\mathbb{R}^n}\,.$$

The notations coincide with those of SubSection 4.1.

As for the best approximation, the test series show, that, if we have a higher degree of absorption, the error decreases up to a certain number M of monomials, then it increases, see Figure 3, Tables 2 and 3. That means, that we must choose the number of basis functions carefully, if we have some absorption within the object.

Remark 4.1. The reason for the large inaccuracy in the case of approximate inverse is the following: We consider the ERT as mapping between $L_2(B)$ and $L_2(S^1\times S^1)$, so we have a weakly ill-posed problem for $\varepsilon_0 \neq 0$. However in case of best approximation we consider the ERT as operator between the Sobolev spaces $H^1(B)$ and $H^1(S^1\times S^1)$, which are endowed with a weaker topology. Now, the ERT is a bounded operator, see (3.1), with a continuous inverse between the spaces $H^1(S^1\times S^1)$ and $L_2(B)$, see (2.5), represented by (3.27). Thus, in this situation we have an approximation to a continuous operator and the high accuracy may not surprise. The weakly ill-posedness of I^{ε_0} was proved in [4].

4.3 Tomography problem with refraction in a medium

The third series of tests is performed for an investigation of a distorting influence of the refraction on the reconstruction accuracy. We remind that the data are

	Best Approximation						Appr. Inv.	
sst M	12 91	13 105	14 120	15 136	16 153	17 171	γ	
$\varepsilon_0 = 0$	0.151	0.063	0.017	0.008	0.001	0.001	0.02	6.34
$\varepsilon_0 = 1$	0.120	0.049	0.013	0.006	0.001	0.001	0.016	32.98
$\varepsilon_0 = 2$	0.118	0.047	0.012	0.005	0.006	0.006	0.016	54.51
$\varepsilon_0 = 3$	0.128	0.051	0.015	0.012	0.013	0.023	0.016	69.55
$\varepsilon_0 = 5$	0.158	0.061	0.071	0.086	0.163	0.235	0.017	85.20
$\varepsilon_0 = 0$	1.87	1.40	0.67	0.35	0.29	0.13	0.02	7.41
$\varepsilon_0 = 1$	1.577	1.199	0.586	0.307	0.260	0.194	0.016	41.08
$\varepsilon_0 = 2$	1.528	1.142	0.545	0.267	0.265	0.213	0.016	64.21
$\varepsilon_0 = 3$	1.605	1.235	0.580	0.315	0.642	0.743	0.016	78.60
$\varepsilon_0 = 5$	2.001	1.620	1.729	1.695	2.827	2.860	0.018	92.11

Table 2: Relative errors in % in the reconstructions of the source functions (F.1–F.2) from the ERT with different constant absorptions ε_0 by the best approximation and the approximate inverse (right column) with $N = 64$

	Best Approximation						Appr. Inv.	
sst M	12 91	13 105	14 120	15 136	16 153	17 171	γ	
$\varepsilon_0 = 0$	5.56	4.56	3.51	2.28	1.89	0.94	0.02	8.04
$\varepsilon_0 = 1$	5.17	4.06	3.09	2.02	1.67	1.17	0.016	37.14
$\varepsilon_0 = 2$	5.18	3.99	2.99	1.79	1.96	1.88	0.016	58.92
$\varepsilon_0 = 3$	5.28	4.12	3.02	1.94	5.36	6.20	0.016	74.11
$\varepsilon_0 = 5$	5.67	4.57	7.13	7.48	16.44	17.73	0.018	90.41
$\varepsilon_0 = 0$	23.52	20.56	17.10	12.37	11.28	6.91	0.02	14.12
$\varepsilon_0 = 1$	22.28	18.70	15.52	11.31	10.17	8.11	0.016	44.35
$\varepsilon_0 = 2$	22.38	18.61	15.31	10.19	11.74	11.08	0.016	65.87
$\varepsilon_0 = 3$	22.76	19.19	15.47	10.69	28.64	32.39	0.016	79.63
$\varepsilon_0 = 5$	24.24	21.06	30.32	31.97	64.88	71.73	0.018	93.19

Table 3: Relative errors in % in the reconstruction of the source functions (F.3–F.4) from the ERT with different constant absorptions ε_0 by the best approximation and the approximate inverse (right column) with $N = 64$

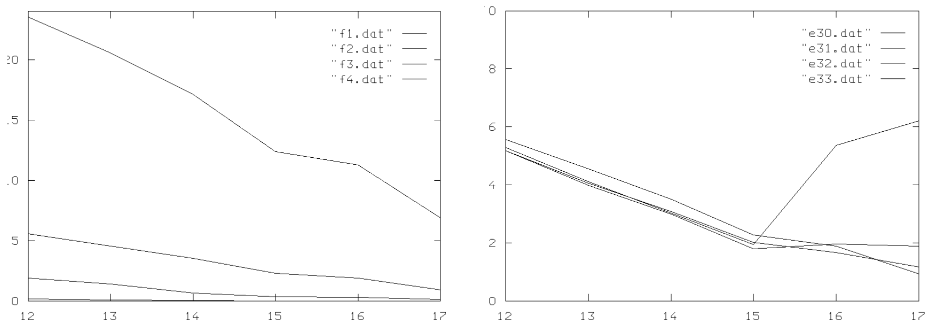

Figure 3: Reconstruction accuracies (in %) of the source functions (F.1–F.4) (left), see Table 1, and (F.3) (right), see Table 3, depending on the maximum degree sst of the approximating polynomial. As data we used on the left side the X-ray transform of the functions, and the ERT with constant absorption $\varepsilon_0 = 0, 1, 2, 3$ on the right side, respectively. In both situations we applied the algorithm of best approximation

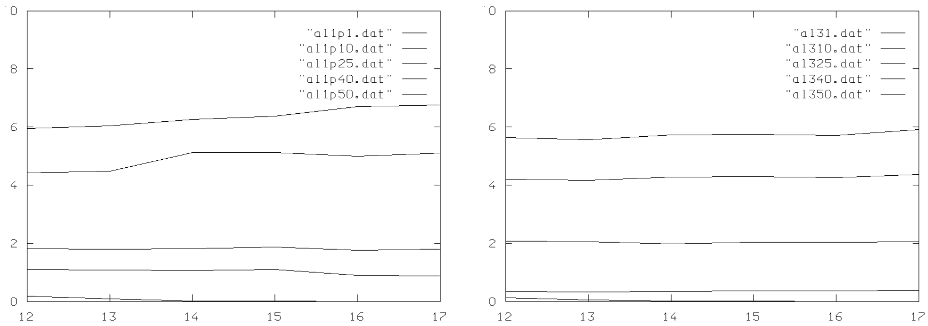

Figure 4: Relative reconstruction errors (in %) of the source function (F.1) in a medium with different degrees of refraction. The refraction is modeled by the CCP-metric (left) and the CCN-metric (right), respectively. The parameter a characterizing the mean curvature was chosen as $a = 0.1, 0.25, 0.4, 0.5$. The reconstruction was performed by the algorithm of best approximation under the assumption that the rays in the medium are straight lines

computed in a case of a medium with refraction. More precisely, the data are ray integrals along geodesics of given Riemannian metrics with positive and negative curvatures and different values of mean curvature a^2. Then we recover the source functions under the assumption that the rays are straight lines.

The formula for the ray transform has the general form (2.3) with $\varepsilon \equiv 0$ in this case,

$$If(x,\xi) = \int_{\tau_-(x,\xi)}^{0} f(\gamma_{x,\xi}(t))\ \mathrm{d}t. \tag{4.5}$$

As for the notations x, ξ, $\gamma_{x,\xi}$ and $\tau_-(x,\xi)$ see Section 2.

Step 1 (Direct problem). We calculate the ray transform of the function $f(x,y)$ along geodesic lines of a fixed metric (see Appendix A.2) using the system of differential equations (G.1) at the points $(k\Delta\alpha,\ \beta_0 - l\Delta\beta)$, $k = 0, 1, \dots, N-1$, $\beta_0 = \pi/2$, $l = 1, 2, \dots, N/2 - 1$, $\Delta\alpha = \Delta\beta = 2\pi/N$.

Step 2 (Inverse problem I). For comparing the influence of refraction, we reconstruct at first the source function $f(x,y)$ with the algorithm of best approximation by its known ray transform along geodesic lines of a given Riemannian metric. The metric is characterized by the parameter a, which we choose equal to 1. In this case we approximate in fact the inversion of the operator I given in (4.5). The results are located in the first line of each table.

Step 3 (Inverse problem II) We reconstruct the function $f(x,y)$ from its known ray transform I along geodesic lines under the assumption that the rays are straight lines. With the numerical experiments we want to investigate the behaviour of the reconstruction error, if the derivation of the rays away from straight lines increases. We apply both, the algorithm of approximate inverse and the algorithm of least squares. In all computations we set $N = 64$.

Tables and results of the tests. As can easily be seen, the metrics (M.2–M.3) with constant positive (negative) curvature are equal to the euclidean one, if $R = 2$, $a = 0$. In all numerical tests, if we use the metrics (M.3) or (M.4), the first parameter R is fixed and equal to 2.

Below there are four groups of tables for the functions (F.1–F.4). Every group contains two tables with the results of numerical tests for the metrics (M.2–M.3). The first line of every table contains the reconstruction accuracy according to Step 2.

5. CONCLUSION AND DISCUSSION

An inclusion of refraction into the mathematical model restricts the mathematical tools, which are usually applied in computerized tomography, essentially. Some important theorems, as for example the center slice theorem, are no longer valid. This implies, that we must think about new numerical methods.

In particular there are not so many numerical methods for solving the emission tomography problem for a medium with arbitrary varying absorption and refraction. In this case there are no inversion formulas, and no results

	Best Approximation						Appr. Inv.	
sst M	12 91	13 105	14 120	15 136	16 153	17 171	γ	
$a = 1.0$	0.179	0.078	0.018	0.008	0.002	0.001	—	—
$a = 0.10$	1.10	1.08	1.06	1.09	0.89	0.88	0.02	6.48
$a = 0.25$	1.81	1.80	1.82	1.87	1.76	1.79	0.02	6.79
$a = 0.40$	4.43	4.47	5.13	5.12	4.99	5.10	0.02	7.82
$a = 0.50$	5.95	6.04	6.26	6.37	6.70	6.76	0.02	9.08
$a = 0.75$	10.48	10.56	11.26	11.31	11.26	11.38	0.021	14.18
$a = 1.00$	15.80	15.81	15.84	15.78	15.96	16.11	0.021	20.37
$a = 1.25$	22.08	22.07	22.02	22.06	22.27	22.40	0.028	24.99
$a = 1.50$	28.28	28.25	27.92	28.01	28.30	28.44	0.037	29.55
$a = 1.75$	36.32	36.37	35.16	35.13	35.26	35.48	0.046	33.68

Table 4: Relative errors in % in the reconstruction of the source function (F.1) according to the Steps 1 and 2. The rays are geodesics of the CCP-metric with $R = 2$ and different values of the parameter a, see also the appendix. At the left hand we have the results of the best approximation, the approximate inverse is located at the right column with $N = 64$

	Best Approximation						Appr. Inv.	
sst M	12 91	13 105	14 120	15 136	16 153	17 171	γ	
$a = 1.0$	0.131	0.055	0.015	0.006	0.001	0.001	—	—
$a = 0.10$	0.35	0.32	0.35	0.36	0.37	0.38	0.02	6.33
$a = 0.25$	2.08	2.05	1.98	2.04	2.04	2.05	0.02	6.28
$a = 0.40$	4.20	4.17	4.27	4.29	4.26	4.36	0.02	6.75
$a = 0.50$	5.64	5.56	5.72	5.74	5.71	5.91	0.02	7.72
$a = 0.75$	11.66	11.57	12.21	12.50	13.04	13.38	0.02	12.94
$a = 1.00$	17.98	17.99	18.48	18.79	19.55	19.84	0.02	20.20
$a = 1.25$	24.77	25.10	26.21	26.10	25.27	25.45	0.02	26.38
$a = 1.50$	32.11	32.83	33.91	33.78	31.77	32.40	0.057	32.98
$a = 1.75$	41.61	41.97	43.67	43.68	39.92	39.86	0.068	36.12

Table 5: Relative errors in % in the reconstruction of the source function (F.1) according to the Steps 1 and 2. The rays are geodesics of the CCN-metric with $R = 2$ and different values of the parameter a, see also the appendix. At the left hand we have the results of the best approximation, the approximate inverse is located at the right column with $N = 64$

	Best Approximation						Appr. Inv.	
sst M	12 91	13 105	14 120	15 136	16 153	17 171	γ	
$a = 1.0$	2.149	1.616	0.699	0.381	0.299	0.132	—	—
$a = 0.10$	1.88	1.51	0.84	0.65	0.63	0.61	0.02	7.50
$a = 0.25$	2.91	2.76	2.50	2.47	2.52	2.64	0.02	8.21
$a = 0.40$	6.07	6.25	6.23	6.22	6.30	6.63	0.02	10.30
$a = 0.50$	9.52	9.66	9.59	9.67	9.88	10.47	0.02	12.67
$a = 0.75$	20.92	21.16	21.15	21.23	21.32	22.44	0.02	21.63
$a = 1.00$	35.74	36.19	36.27	36.28	36.41	37.57	0.02	33.37
$a = 1.25$	51.29	51.77	51.94	51.75	51.63	52.50	0.021	46.01
$a = 1.50$	66.56	66.67	67.14	66.73	66.91	67.09	0.065	55.01

Table 6: Relative errors in % in the reconstruction of the source function (F.2) according to the Steps 1 and 2. The rays are geodesics of the CCP-metric with $R = 2$ and different values of the parameter a, see also the appendix. At the left hand we have the results of the best approximation, the approximate inverse is located at the right column with $N = 64$

	Best Approximation						Appr. Inv.	
sst M	12 91	13 105	14 120	15 136	16 153	17 171	γ	
$a = 1.0$	1.720	1.300	0.615	0.313	0.258	0.162	—	—
$a = 0.10$	1.91	1.44	0.82	0.58	0.53	0.47	0.02	7.34
$a = 0.25$	3.07	2.86	2.74	2.67	2.69	2.74	0.02	7.24
$a = 0.40$	6.93	6.85	6.79	6.77	6.88	7.17	0.02	8.38
$a = 0.50$	10.34	10.26	10.21	10.20	10.37	10.83	0.02	10.55
$a = 0.75$	23.39	22.99	23.17	23.28	23.60	24.44	0.02	21.28
$a = 1.00$	41.83	40.20	40.53	40.79	41.15	42.41	0.02	38.32
$a = 1.25$	62.14	59.50	60.79	61.27	63.30	64.14	0.065	53.76
$a = 1.50$	79.55	78.38	80.17	80.80	82.26	82.37	0.092	69.72

Table 7: Relative errors in % in the reconstruction of the source function (F.2) according to the Steps 1 and 2. The rays are geodesics of the CCN-metric with $R = 2$ and different values of the parameter a, see also the appendix. At the left hand we have the results of the best approximation, the approximate inverse is located at the right column with $N = 64$

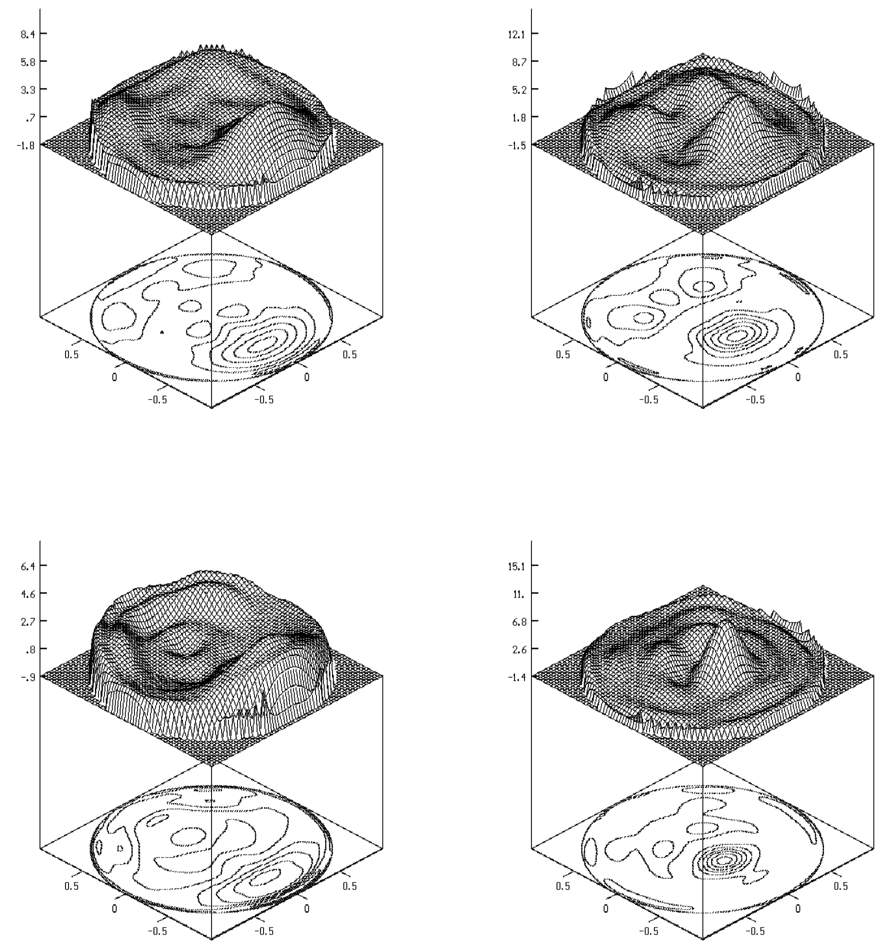

Figure 5: Reconstructions of (F.2) with the method of best approximation according to Step 2 using the CCP-metric (left side) and the CCN-metric (right side). The parameter a was chosen as $a = 1.0$ (upper pictures) and $a = 1.5$ (lower pictures), respectively. These choices mean a strong degree of deflection. As for the accuracies see the Tables 8 and 9

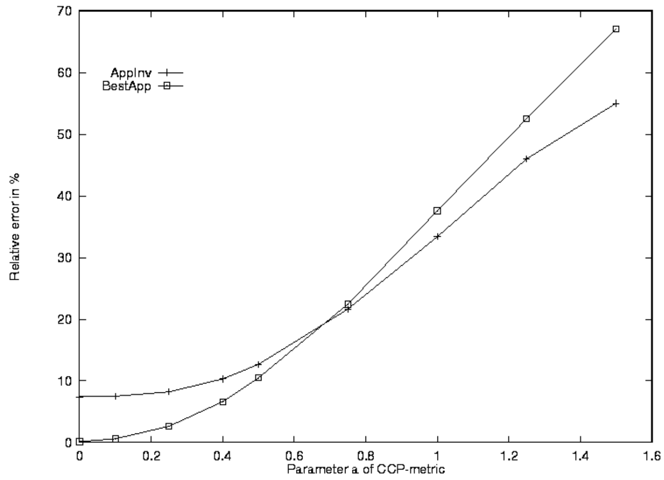

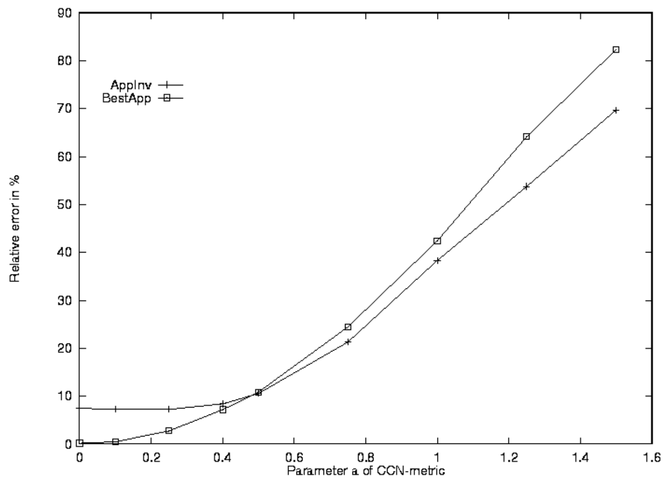

Figure 6: Reconstruction accuracies for (F.2). Comparison of both algorithms where the refraction is modeled by the CCP-metric (top) and the CCN-metric (bottom), respectively. We see, that the approximate inverse (marked by crosses) achieves better results for large refractions, whereas the best approximation (marked by squares) is more exact, if the deflections are small

	Best Approximation						Appr. Inv.	
sst	12	13	14	15	16	17	γ	
M	91	105	120	136	153	171		
$a = 1.0$	6.035	4.827	3.766	2.457	1.973	0.999	—	—
$a = 0.10$	5.58	4.58	3.53	2.30	1.97	1.16	0.02	8.10
$a = 0.25$	5.88	4.97	4.09	3.26	3.09	2.88	0.02	8.71
$a = 0.40$	8.10	7.62	7.06	6.69	6.66	6.84	0.02	10.82
$a = 0.50$	11.42	10.93	10.31	10.20	10.24	10.64	0.02	13.36
$a = 0.75$	22.59	22.25	21.87	21.91	21.84	22.27	0.02	23.00
$a = 1.00$	36.09	35.84	35.66	35.98	35.86	35.81	0.02	35.04
$a = 1.25$	48.85	48.69	48.73	49.07	48.84	48.93	0.048	46.03
$a = 1.50$	61.83	61.98	62.43	62.56	62.20	62.14	0.074	53.82

Table 8: Relative errors in % in the reconstruction of the source function (F.3) according to the Steps 1 and 2. The rays are geodesics of the CCP-metric with $R = 2$ and different values of the parameter a, see also the appendix. At the left hand we have the results of the best approximation, the approximate inverse is located at the right column with $N = 64$

	Best Approximation						Appr. Inv.	
sst	12	13	14	15	16	17	γ	
M	91	105	120	136	153	171		
$a = 1.0$	5.395	4.262	3.296	2.124	1.710	1.029	—	—
$a = 0.10$	5.60	4.60	3.57	2.53	1.92	0.99	0.02	8.00
$a = 0.25$	6.19	5.34	4.46	3.60	3.28	2.90	0.02	8.12
$a = 0.40$	8.70	8.25	7.76	7.56	7.43	7.46	0.02	9.77
$a = 0.50$	11.60	11.46	11.11	11.18	11.08	11.26	0.02	13.38
$a = 0.75$	24.34	24.56	24.46	25.04	24.90	25.28	0.02	23.99
$a = 1.00$	42.23	42.64	42.53	42.90	42.56	43.97	0.04	39.96
$a = 1.25$	61.87	61.93	61.53	61.79	62.74	64.51	0.062	54.18
$a = 1.50$	76.47	75.47	75.03	75.47	77.52	78.46	0.152	65.87

Table 9: Relative errors in % in the reconstruction of the source function (F.3) according to the Steps 1 and 2. The rays are geodesics of the CCN-metric with $R = 2$ and different values of the parameter a, see also the appendix. At the left hand we have the results of the best approximation, the approximate inverse is located at the right column with $N = 64$

	Best Approximation						Appr. Inv.	
sst	12	13	14	15	16	17	γ	
M	91	105	120	136	153	171		
$a = 1.0$	24.74	22.03	18.42	13.11	11.56	7.29	—	—
$a = 0.10$	23.52	20.55	17.07	12.33	11.27	6.99	0.02	14.19
$a = 0.25$	23.70	20.61	17.28	12.69	11.78	8.08	0.02	14.95
$a = 0.40$	24.83	21.81	19.16	14.79	13.97	12.00	0.02	17.68
$a = 0.50$	27.05	24.04	21.68	17.83	17.29	16.74	0.02	21.07
$a = 0.75$	38.16	35.85	34.03	32.73	32.39	33.15	0.02	33.77
$a = 1.00$	53.75	52.57	51.95	51.48	50.95	50.02	0.02	48.00
$a = 1.25$	67.69	66.99	67.10	66.75	66.20	66.40	0.021	58.98
$a = 1.50$	79.88	79.49	80.36	79.90	79.84	80.02	0.05	66.58

Table 10: Relative errors in % in the reconstruction of the source function (F.4) according to the Steps 1 and 2. The rays are geodesics of the CCP-metric with $R = 2$ and different values of the parameter a, see also the appendix. At the left hand we have the results of the best approximation, the approximate inverse is located at the right column with $N = 64$

	Best Approximation						Appr. Inv.	
sst	12	13	14	15	16	17	γ	
M	91	105	120	136	153	171		
$a = 1.0$	22.76	19.62	16.46	11.80	10.39	7.39	—	—
$a = 0.10$	23.54	20.63	17.17	12.42	11.29	6.88	0.02	14.08
$a = 0.25$	23.95	21.27	17.81	13.38	12.00	7.82	0.02	14.30
$a = 0.40$	25.74	23.44	20.35	17.03	15.83	12.78	0.02	16.56
$a = 0.50$	28.24	26.39	23.70	21.52	20.58	18.18	0.02	20.13
$a = 0.75$	40.87	40.63	39.15	39.21	38.58	37.47	0.02	36.03
$a = 1.00$	60.37	61.60	60.91	61.18	60.46	61.74	0.041	53.67
$a = 1.25$	83.04	83.36	82.40	82.29	83.40	84.96	0.055	65.78
$a = 1.50$	95.53	94.38	92.83	92.94	95.00	97.28	0.086	76.70

Table 11: Relative errors in % in the reconstruction of the source function (F.4) according to the Steps 1 and 2. The rays are geodesics of the CCN-metric with $R = 2$ and different values of the parameter a, see also the appendix. At the left hand we have the results of the best approximation, the approximate inverse is located at the right column with $N = 64$

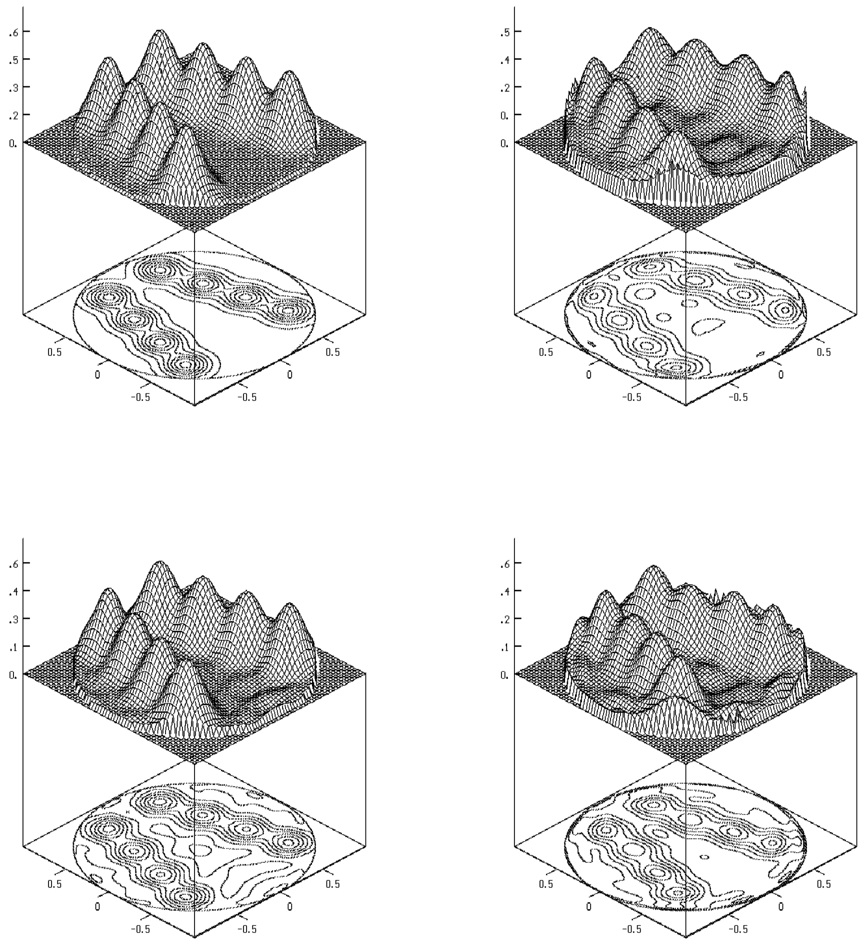

Figure 7: Source function (F.4) (top left) and its reconstruction according to Step 1 (bottom left). To the right side we have the reconstructions of (F.4) according to Step 2 using the CCP-metric (top) and the CCN-metric (bottom), respectively. In both cases the parameter a was chosen as $a = 0.75$. As for the accuracies, see the Tables 10 and 11. The reconstructions were produced with the method of best approximation

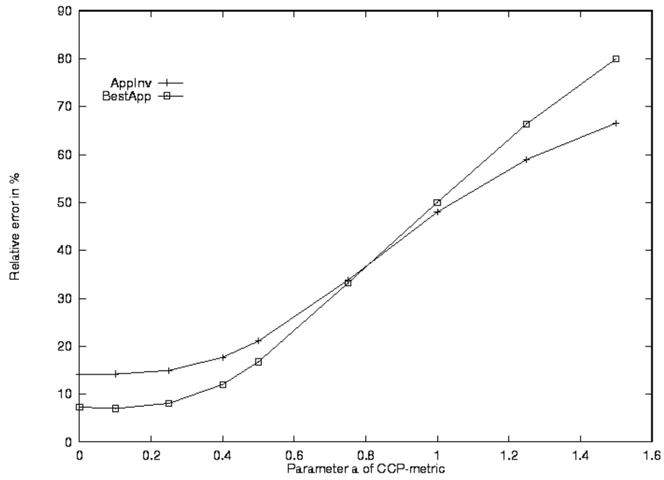

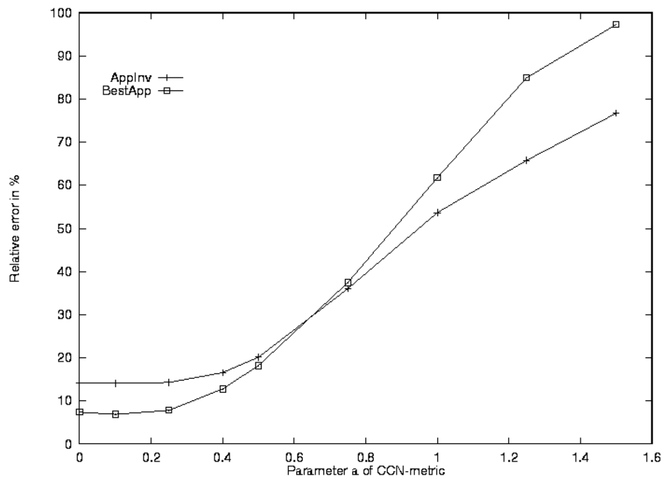

Figure 8: Reconstruction accuracies for (F.4). Comparison of both algorithms where the refraction is modeled by the CCP-metric (top) and the CCN-metric (bottom), respectively. In this drawing the effect from Figure 7 becomes even more obviousely: The approximate inverse (marked by crosses) achieves better results for large refractions, whereas the best approximation (marked by squares) is more exact, if the refractions are small

analogous to the center slice theorem. The latter makes an employment with the wide collection of algorithms for traditional tomography problems, which bases on these two main results, impossible. At present the variational methods seem to be the only class of methods appropriate for the solution of this complicated problem.

If we want to use a more coincident model in order to obtain more precise results, then the following questions arise in a natural way:

1) Is it possible to answer the question whether there exists a refraction within the medium or not by using the input data, that means the ray integrals of the source function, only and without any a priori information about the medium?

2) If there is a refraction within the medium, is it reasonable to include a Riemannian metric into the mathematical model? As we mentioned above this would have consequences for the mathematical tools we want to apply.

3) Let us suppose, that the answer to the first two questions is positive, then the question arises, if the data for solving the two following problems are complete: The problem of determining an unknown Riemannian metric by some data and the reconstruction of the source function by using the information about the metric, which we have obtained by solving the first problem.

The numerical results in Section 4, where we tested the two algorithms, give some answers to question 2).

a) Even under the condition of a strong refraction ($a = 1.0$) the algorithm of least squares reconstructs the source functions almost with the same accuracy as in the first series of tests, see Table 1.

b) If we have a high accuracy in the reconstruction, see Tables 4–7 (first line), then even a very small level of refraction, for example with mean curvature $a^2 < 0.01$, leads to a large increase of the errors. For the functions (F.3–F.4) a weak refraction, for example with mean curvature $a^2 < 0.0625$, causes only a small increase of the errors. We remind that in the first set of tests the functions (F.3–F.4) were recovered with an accuracy of 0.94%, 6.91%, respectively.

c) A typical behaviour of the reconstruction accuracies with the method of best approximation is the following: The error decreases up to a certain number of basis functions, after that it increases, see Figure 3. That means, that the choice of the number M of basis functions must be handled carefully. It represents a regularization parameter.

d) The question, whether we take the best approximation, or the approximate inverse as reconstruction method, depends also on the refraction level. We have seen, that the method of approximate inverse has advantages in accuracy, if the refraction level is large, see Figures 6 and 8.

e) In any case, as for the efficiency, the approximate inverse must be emphasized in opposite to the best approximation.

f) We remind that the numerical tests with the method of best approximation show a very different behaviour of the error with respect to the degree of the basis functions, see Figures 3 and 4, respectively. More precisely, if the level of absorption or deflection increases, then a diagram, where we draw the error versus the degree of polynomial, has a form, which is typical for ill-posed problems, see Figures 3,4, Tables 2 and 3: From a certain value sst the relative error increases significantly. On the contrary the influence of absorption leads to a nearly constant relative error. Nevertheless this error is large.

g) A draw-back of the method of best approximation is that the searched-for function is projected in the H^1-scalar product to smooth functions spanned by the monomials. The reconstructions tend to produce smooth approximations, where small objects are practically invisible. This was already observed by Logan – Shepp, see [5].

The results of Subsection 4.3 give also approaches to the problems which are mentioned in question 3). If we want to reconstruct the source function very precisely, then the inclusion of a refraction, if there is any, into the model allows us to increase the accuracy of the reconstruction considerably, see Tables 4–7. The situation is the same, if there exists a sufficiently strong refraction with curvatures $a^2 > 0.1$, see Tables 4–11, Figure 7, on the right side. If our purpose is to recover main properties of the source function only, and the level of refraction is not so strong, then there is no sense in using the tools of Riemannian geometry.

An example for a field, where refractions play an important role, are seismic problems. It is a well known fact, that in the topic of seismics the refraction is so strong, that the questions 1) and 2) do not arise at all. Moreover the refraction of elastic waves is the main and maybe the only tool to obtain the data for solving the principal seismic problems. In particular we mean kinematic and dynamic seismic problems. The data information for these problems are different. More exactly, the data (times of signal running, or lengths of rays in the sense of certain Riemannian metric in a ray terminology) for the kinematic problem may be contained in the data for the dynamic one. Thus, for researches in seismic topic there is no doubt, that special information is necessary in order to find the solution of the kinematic problem. Note, that the "refraction tomography problem" with unknown Riemannian metric, which is analogous to the dynamic problem of seismics by its main properties, has a very big degree of nonuniqueness.

Starting from the foregoing observations, we suggest the following algorithm for detecting the type of refraction and give a possible answer to question 1):

a) We reconstruct the source function along straight lines using the algorithm of best approximation or approximate inverse and calculate the residuum

$$\|g - g_{\mathrm{app}}\| \,. \tag{5.1}$$

Here, g denotes our measured data, and $g_{\mathrm{app}} = I f_{\mathrm{app}}$ are data computed with our approximated solution f_{app}. As a norm we can take the L_2-norm for example. Our aim is to determine a metric in the representation (4.5) of I such that the norm (5.1) is minimized.

b) We repeat Step a) introducing a set of Riemannian metrics of constant positive, or negative curvature (CCP-, CCN-metric). We start with a small value of the parameter a characterizing the CCP- and CCN-metric, and use this metric instead of the euclidean one in the representation (4.5) of I.

c) Starting with $a = 0.1$ for example we increase this value and compute the residuum (5.1) each time.

d) If there exists a parameter a, and hence a value of positive or negative curvature, for which the norm (5.1) becomes significantly smaller than in Step a), we have an indirect hint on the presence of any refraction within the object under consideration.

Note, that we must handle carefully with the degree of polynomials sst, if we apply the best approximation, and with the regularization parameter γ, if we apply the approximate inverse, respectively. Usually we must calculate (5.1) for several values of sst and γ due to the behaviour of the reconstruction error, which is typical for ill-posed problems.

6. APPENDIX. LIST OF FUNCTIONS AND RIEMANNIAN METRICS

6.1. List of functions

1. The *fast convergent* function,

$$f(x,y) = \sin(7.5x + 3y + 0.75) + \cos(3x + 7.5y - 0.75) + 5\,\exp\{-5x^2 - 5y^2\} + 2. \tag{F.1}$$

2. The *middle convergent* function,

$$f(x,y) = 5\exp\{-8(x-0.5)^2 - 12(y-0.5)^2\} + 5\exp\{-8(x+0.5)^2 - 12(y-0.5)^2\} + 10\exp\{-6x^2 - 15(y+0.5)^2\} \tag{F.2}$$

3. The *low convergent* function,

$$f(x,y) = \sum_{j=1}^{4} 0.6\big[\exp\{-18(x+0.2+0.1j)^2 - 18(y-1.1+0.4j)^2\} + \exp\{-18(x-0.2-0.1j)^2 - 18(y-1.1+0.4j)^2\}\big]. \tag{F.3}$$

4. The *very low convergent* function,

$$f(x,y) = \sum_{j=1}^{4} 0.6\big[\exp\{-32(x+0.2+0.1j)^2 - 32(y-1.1+0.4j)^2\} + \exp\{-32(x-0.2-0.1j)^2 - 32(y-1.1+0.4j)^2\}\big]. \tag{F.4}$$

Remark A.1. The classification of convergence speed refers to the corresponding Taylor series. Denoting with c_{16} the coefficient of x^{16} in the Taylor series we say, that a function is

— fast convergent, if $|c_{16}| < 1$,

— middle convergent, if $1 \le |c_{16}| \le 100$,

— low convergent, if $|c_{16}| \ge 100$.

For all functions (F.1)–(F.4) we have $f \in C^\infty(B)$.

6.2. List of Riemannian metrics

The square of the length element of any Riemannian metric with fundamental tensor (g_{ij}) is defined by

$$\mathrm{d}s^2 = g_{ij}\,\mathrm{d}x^i\,\mathrm{d}x^j \equiv g_{11}\,\mathrm{d}x^2 + 2g_{12}\,\mathrm{d}x\,\mathrm{d}y + g_{22}\,\mathrm{d}y^2. \tag{M.0}$$

For geodesic lines of a Riemannian metric in the two-dimensional case the system of equations

$$\left.\begin{aligned} \frac{\mathrm{d}^2x}{\mathrm{d}s^2} + \Gamma^1_{11}\Big(\frac{\mathrm{d}x}{\mathrm{d}s}\Big)^2 + 2\Gamma^1_{12}\frac{\mathrm{d}x}{\mathrm{d}s}\frac{\mathrm{d}y}{\mathrm{d}s} + \Gamma^1_{22}\Big(\frac{\mathrm{d}y}{\mathrm{d}s}\Big)^2 = 0 \\ \frac{\mathrm{d}^2y}{\mathrm{d}s^2} + \Gamma^2_{11}\Big(\frac{\mathrm{d}x}{\mathrm{d}s}\Big)^2 + 2\Gamma^2_{12}\frac{\mathrm{d}x}{\mathrm{d}s}\frac{\mathrm{d}y}{\mathrm{d}s} + \Gamma^2_{22}\Big(\frac{\mathrm{d}y}{\mathrm{d}s}\Big)^2 = 0 \end{aligned}\right\} \tag{G.1}$$

is valid, where Γ^k_{ij} are Cristoffel's symbols, and the parameter s of a geodesic line is proportional to its length.

We set a Riemanian metric in a circle of radius R (usually $R = 1$), and denote $r^2 = x^2 + y^2$. The fundamental tensor of conformal metrics (in particular IZT - metric) has the components $g_{11}(x, y) = g_{22}(x, y) \equiv n(x, y)$, $g_{12}(x, y) \equiv 0$, and Cristoffel's symbols

$$\begin{aligned} &\Gamma^1_{11} = \frac{1}{2n}\frac{\partial n}{\partial x}, \quad &\Gamma^1_{12} = \frac{1}{2n}\frac{\partial n}{\partial y}, \quad &\Gamma^1_{22} = -\frac{1}{2n}\frac{\partial n}{\partial x} \\ &\Gamma^2_{11} = -\frac{1}{2n}\frac{\partial n}{\partial y}, \quad &\Gamma^2_{12} = \frac{1}{2n}\frac{\partial n}{\partial x}, \quad &\Gamma^2_{22} = \frac{1}{2n}\frac{\partial n}{\partial y} \end{aligned} \tag{Cr.1}$$

The Gaussian curvature of a conformal metric is given by the formula

$$K = -\frac{1}{2n(x, y)}\,\Delta \ln n(x, y)$$

where $\Delta \equiv \partial^2/\partial x^2 + \partial^2/\partial y^2$ is the Laplacian. We use the first four metrics of the following list in numerical tests.

1. Eucledian metric is defined (as usually) by the following element of length

$$\mathrm{d}s^2 = \mathrm{d}x^2 + \mathrm{d}y^2. \tag{M.1}$$

All Cristoffel's symbols and the Gaussian curvature of the Euclidean metric are equal to zero.

2. A Riemanian metric with *constant positive curvature (CCP-metric)* is defined by the following components of the fundamental tensor

$$g_{11}(x,y) = g_{22}(x,y) \equiv n(x,y) = \frac{4R^2}{(R^2 + a^2r^2)^2} \quad \text{with } a^2 < R^2 . \tag{M.2}$$

Cristoffel's symbols are of the form

$$\Gamma^1_{11} = -\frac{2a^2x}{(R^2+a^2r^2)^2}, \quad \Gamma^1_{12} = -\frac{2a^2y}{(R^2+a^2r^2)^2}, \quad \Gamma^1_{22} = \frac{2a^2x}{(R^2+a^2r^2)^2}$$
$$\Gamma^2_{11} = \frac{2a^2y}{(R^2+a^2r^2)^2}, \quad \Gamma^2_{12} = -\frac{2a^2x}{(R^2+a^2r^2)^2}, \quad \Gamma^2_{22} = -\frac{2a^2y}{(R^2+a^2r^2)^2}. \tag{Cr.2}$$

The Gaussian curvature of the CCP-metric is constant $K = a^2$.

3. The fundamental tensor of a Riemannian metric with *constant negative curvature (CCN-metric)* is written in the form

$$g_{11}(x,y) = g_{22}(x,y) \equiv n(x,y) = \frac{4R^2}{(R^2 - a^2r^2)^2} \quad \text{with } a^2 < R^2 . \tag{M.3}$$

The Cristoffel's symbols have the form

$$\Gamma^1_{11} = \frac{2a^2x}{(R^2-a^2r^2)^2}, \quad \Gamma^1_{12} = \frac{2a^2y}{(R^2-a^2r^2)^2}, \quad \Gamma^1_{22} = -\frac{2a^2x}{(R^2-a^2r^2)^2}$$
$$\Gamma^2_{11} = -\frac{2a^2y}{(R^2-a^2r^2)^2}, \quad \Gamma^2_{12} = \frac{2a^2x}{(R^2-a^2r^2)^2}, \quad \Gamma^2_{22} = \frac{2a^2y}{(R^2-a^2r^2)^2}. \tag{Cr.3}$$

The Gaussian curvature of CCP-metric is constant $K = -a^2$.

REFERENCES

1. M. Abramowitz and I. Stegun, *Handbook of mathematical functions.* Dover, New York, 1972.

2. E. Y. Derevtsov, A. G. Kleshchev, and V. A. Sharafutdinov, Numerical solution of the emission 2D-tomography problem for a medium with absorption and refraction. *J. Inv. Ill-Posed Problems* (1999) **7**, No. 1, 83–103.

3. I. Gradshtein and I. Ryzhik, *Table of integrals series and products.* Academic Press, New York, 1980.

4. I. Hazou and D. C. Solmon, Filtered-backprojection and the exponential radon-transform. *J. Math. Anal. and Appl.* (1989) **141**, 109–119.

5. B. F. Logan and L. A. Shepp, Optimal reconstruction of a function from its projections. *Duke Math. J.* (1975), 645–659.

6. A. K. Louis, Approximate inverse for linear and some nonlinear problems. *Inverse Problems* (1996) **12**, 175–190.

7. A. K. Louis, A unified approach to regularization methods for linear ill-posed problems. *Inverse Problems* (1999) **15**, 489–498.

8. F. Natterer, *The Mathematics of Computerized Tomography.* Wiley, Chichester, 1986.

9. A. Rieder and T. Schuster, The approximate inverse in action with an application to computerized tomography. *SIAM J. Num. Anal.* (1999) (to appear).

10. V. A. Sharafutdinov, *Integral Geometry of Tensor Fields.* Utrecht, VSP, 1994.